Journal of the Mechanical Behavior of Biomedical Materials 172 (2025) 107160

Contents lists available at ScienceDirect

Journal of the Mechanical Behavior of Biomedical Materials

journal homepage: www.elsevier.com/locate/jmbbm

Morpho-mechanical analysis of porcine growth plate tissue mechanics under torsional shear

L. Hucke [a,b,c], G.Q. Teixeira [d], A. Seitz [d], A.J. Gámez [b], A. Huß [a], N. Hammer [c,e,f], A. Wittek [a,*], J.A. Niestrawska [c,**]

[a] Personalized Biomedical Engineering Laboratory, Department 2: Computer Science and Engineering, Frankfurt University of Applied Sciences, Frankfurt, Germany
[b] Department of Mechanical Engineering and Industrial Design, School of Engineering, Universidad de Cádiz, Cádiz, Spain
[c] Division of Macroscopic and Clinical Anatomy, Gottfried Schatz Research Center, Medical University of Graz, Graz, Austria
[d] Institute of Orthopedic Research and Biomechanics, Ulm University Medical Centre, Ulm, Germany
[e] Department of Orthopaedic and Trauma Surgery, University of Leipzig, Leipzig, Germany
[f] Fraunhofer IWU, Dresden, Germany

ARTICLE INFO

Keywords:
Biomechanics
Failure stress
Growth plate
Material properties
Microstructure analysis
Porcine growth plate
Shear modulus

ABSTRACT

Torsional loading of the growth plate occurs in daily activities and sports and is associated with growth plate fractures. This study aimed to investigate the microstructural and mechanical properties of growth plate tissue under torsional loading, focusing on variations across individuals, growth plate types, and anatomical locations.

A total of 140 samples from three distinct growth plates in five porcine subjects were subjected to cyclic torsion tests followed by ultimate failure testing. Additionally, histological analyses were performed using Movat's pentachrome staining to assess tissue structure.

Mechanical testing revealed significant differences in shear moduli across growth plate types; notably, the proximal femur exhibited a higher primary shear modulus compared to both the distal femur and proximal tibia. Correlation analyses showed a negative relationship between hypertrophic zone thickness and primary shear modulus ($\rho = -0.47$ at $0.5°/s$, $p < 0.001$), as well as between cell column angle and secondary shear modulus ($\rho = -0.43$ at $0.5°/s$, $p = 0.015$).

This study provides essential insights into the mechanical behavior of growth plates and how structural variations influence their response to loading, aiding in the development of more accurate computational models.

1. Introduction

Growth plates, located between the epiphysis and metaphysis, are key sites of longitudinal bone growth and consist of specialized cartilage arranged in four zones. Stem cells in the resting zone proliferate and align in columns, enlarge in the hypertrophic zone, and under hypoxic stress, trigger matrix calcification, leading to continuous bone translocation (D'Andrea et al., 2021). Collagen type II distribution varies across zones, aligning with cell columns in the hypertrophic and proliferative zones, and perpendicular in the resting zone (Amini et al., 2012; Eckstein et al., 2022). Mechanical loading plays a fundamental role in stem cell differentiation and growth plate adaptation (Zhang et al., 2022; Stamos and Berthaume, 2021; Stamos and Weaver, 2020; Castro-Abril et al., 2016; Thomson, 1902), forming the basis of treatments like guided growth (Stevens, 2007; Gottliebsen et al., 2013, 2016; Hucke et al., 2023). However, outcomes vary due to complex biomechanical-biological interactions (Stief et al., 2021; Farr et al., 2018), underlining the need to understand growth plate behavior under different loading types.

Material properties of growth plate cartilage are often approximated using linear-elastic, quasi-incompressible models with Young's moduli between 2 and 1000 MPa and Poisson ratios ranging from 0.4 to 0.495 (e.g. Koller et al., 2024; Hucke et al., 2023; Sadeghian et al., 2023; Alonso et al., 2022; Yadav et al., 2016; Carriero et al., 2011) – often without clearly stating the specific point or region of the loading curve from which these values are derived. Further experimental work is

* Corresponding author.
** Corresponding author.
E-mail addresses: wittek@fb2.fra-uas.de (A. Wittek), justyna.niestrawska@medunigraz.at (J.A. Niestrawska).

https://doi.org/10.1016/j.jmbbm.2025.107160
Received 4 February 2025; Received in revised form 1 June 2025; Accepted 11 August 2025
Available online 12 August 2025
1751-6161/© 2025 The Authors. Published by Elsevier Ltd. This is an open access article under the CC BY license (http://creativecommons.org/licenses/by/4.0/).

needed to refine our understanding of how tissue properties vary with factors such as growth plate type, position within the plate, loading conditions (e.g., initial vs. non-linear response), and inter-individual variation.

Previous studies have explored compressive and shear loading in porcine growth plates (Fischenich et al., 2022; D'Andrea et al., 2021; Shen et al., 2020; Wosu et al., 2012; Amini et al., 2012; Sergerie et al., 2009, 2011; Niehoff et al., 2004), but torsional loading remains largely unexplored. Porcine models are widely accepted due to their anatomical and mechanical similarities to human growth plates (Cone et al., 2017). Torsional stresses are highly relevant in sports and daily activities involving quick directional changes (Mirtz et al., 2011). The knee allows 25°–30° of internal/external tibial rotation (Innocenti, 2022), with 4°–8° occurring during normal gait (Perry and Burnfield, 2010). These motions play a role in the screw-home mechanism, contributing to knee stabilization during stance and allowing shock absorption through controlled internal rotation. During such phases, when the limb is dynamically loaded, torsional moments in the femur and tibia can reach 13–48 Nm (Heyland et al., 2023), and even higher in impact sports like basketball or skiing (Giesche et al., 2021), increasing the risk of growth plate injury.

The present study aims to characterize the mechanical and histomorphological properties of growth plate tissue under torsional loading. Specifically, it investigates correlations between mechanical parameters and microstructural features, as well as potential differences between individuals, growth plate types, and locations within the same plate. By explicitly defining the points on the loading curve used to calculate the moduli, our approach helps to better constrain and contextualize the wide range of reported mechanical properties.

2. Materials and methods

2.1. Sample retrieval and processing

The hind limbs from five pigs of unknown gender, each approximately six months old (analogous to human adolescence) (Cone et al.,

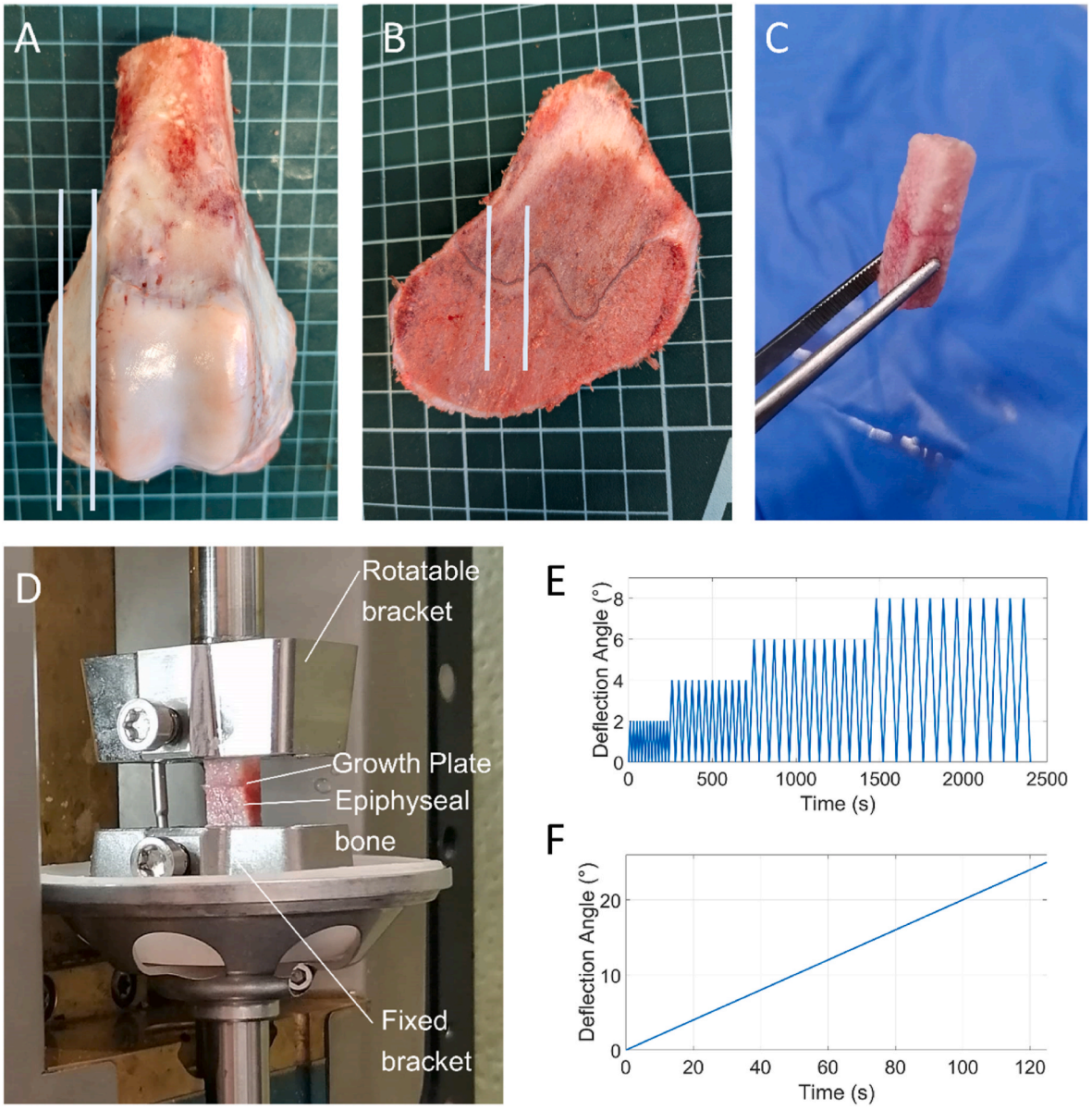

Fig. 1. Sample preparation and testing procedure using the distal femoral growth plate as an example. (A) Distal femur with exemplary cutting lines (gray). (B) 5 mm thick transverse section with cutting lines for sample extraction. (C) Final 5 × 5 × 15 mm sample. (D) Mounted sample in the mechanical testing device. (E) Cyclic loading protocol at 0.2°/s. (F) Continuous loading to failure at 0.2°/s.

2017) were utilized for this study. The tissues were collected from a local butcher within 24 h *post mortem*. The proximal tibia and both the proximal and distal femur were removed for subsequent sampling. Growth plate bone samples measuring approximately 5 × 5 × 15 mm were extracted from each specimen and region, assuring that the growth plate was aligned horizontally within the samples (Fig. 1, A–C). To ensure straight cuts and a consistent sample width, the specimens were secured in a vice that simultaneously served as a cutting guide. A manual handsaw was used to minimize heat generation and prevent thermal damage to the sensitive tissue. For all three growth plate types, samples were classified according to their anatomical location in the transversal plane: medial and lateral (Fig. 2) (Fischenich et al., 2022; Hucke et al., 2023). In consideration of the distinctive morphology of the distal femoral growth plate, a further delineation was made with respect to whether the sampled specimen originates from a valley within its corresponding quadrant (Hucke et al., 2023). The samples were then frozen in a phosphate-buffered saline solution (PBS, pH = 7.4) at −80 °C until further processing.

2.2. Torsion tests

The samples were thawed at 19°C and then mounted in a Rheometer (MCR 702e MultiDrive, Anton Paar Group AG, Graz, Austria). The lower clamp served as a fixed mount, while the upper clamp enabled rotation. The samples were consistently clamped at an 8 mm distance between the clamps (Fig. 1, D), ensuring that the growth plate was positioned at the midpoint. The positioning was aligned manually and subsequently subjected to a visual examination. During the testing, the samples were continuously moistened with PBS. The samples were subjected to cyclic deformation (Fig. 1, E) at three different velocities, ranging from slow (0.04°/s) to medium (0.2°/s) and fast (0.5°/s) (Sun et al., 2022). The samples were loaded with rotations of up to 8° or 10° in 2°-increments (Fig. 1, E). The number of preconditioning cycles (5 cycles for 0.04°/s, 12 cycles for 0.2°/s, 20 cycles for 0.5°/s) was set based on preliminary tests using 15 samples, where the stabilization of maximum moment over time was used as a criterion. After the cyclic tests, each sample was given a 5 min rest period according to Fischenich et al. (2022), before being deformed until failure. The sample was subjected to a continuous deformation up to 25°, using the same testing velocities as in the respective cyclic testing (Fig. 1, F). For the distal femoral growth plate, all specimens were tested at a loading velocity of 0.2°/s. This rate was selected to enable comparison across anatomical subregions within the plate, as originally intended by the experimental design. Due to limited sample availability following specimen exclusion, analysis was restricted to pooled results.

2.3. Evaluation of mechanical tests

In the evaluation of the experimental data, it is assumed that the deformation occurs exclusively in the growth plate tissue. This assumption was made due to the fact that bone is considerably stiffer than the tissue of the growth plate.

All evaluations were carried out using Matlab 2023a (MathWorks, MATLAB, Version R2023a, Natick, Massachusetts, USA). To evaluate the cyclic tests, the torque and angle of rotation were converted as follows into torsional stress τ and shear strain γ. The samples were treated as rectangular in order to account for any deviations from a square shape in the evaluation. The maximal torsional stress τ_{max} was determined as

$$\tau_{max} = \frac{TC}{K}, \tag{1}$$

where T denotes the torque as measured, C is the distance from the center to the outermost fiber, which in this case is the half of the longer side of the rectangle. K is the torsional constant which can be approximated as follows:

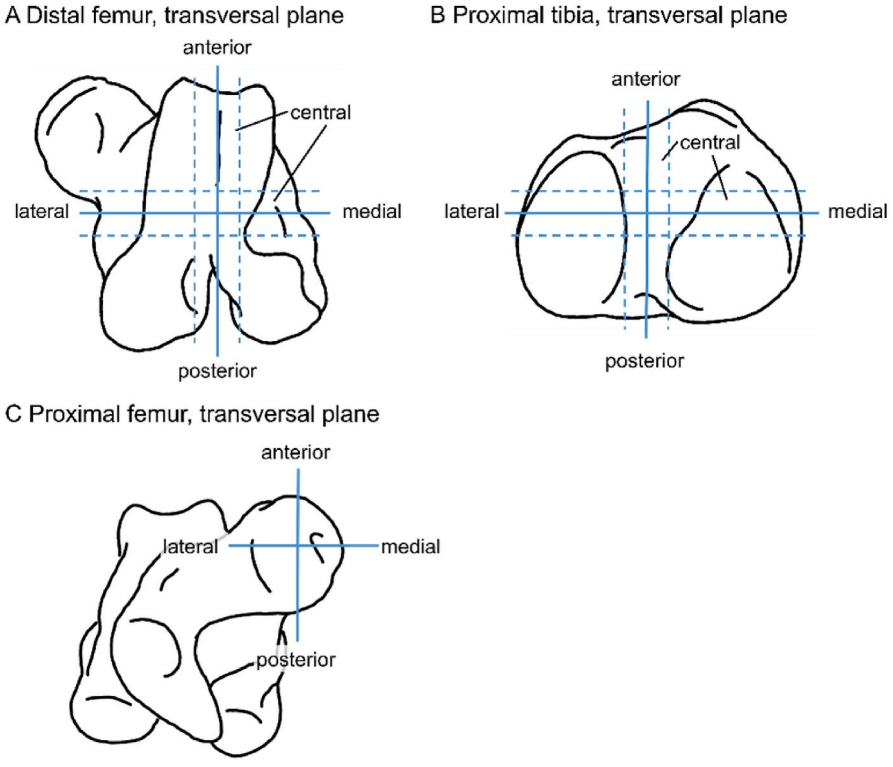

Fig. 2. Assignment of anatomical locations for samples. (A) Distal femur and (B) proximal tibia samples were classified by sagittal (medial–central–lateral) and coronal (anterior–central–posterior) positions. (C) Proximal femur growth plates, due to their smaller size, were divided into lateral-medial-anterior-posterior regions.

$$K \approx ab^3 \left[\frac{16}{3} - 3.36 \frac{b}{a} \left(1 - \frac{b^4}{12a^4} \right) \right], \quad (2)$$

with a being half of the longer and b being half of the shorter side of the rectangular cross section of the sample (Young and Budynas, 2002).

Equations (1) and (2) imply the assumption that the growth plate was plane and perpendicular to the longitudinal axis of the specimen. This did not hold exactly for all specimen, which showed deviations from this ideal geometry: an angle other than 90° to the longitudinal axis and curved form (cf. Fig. 2 of the supplementary material). Following a method similar to Shen et al. (2020), the angle between growth plate and transversal plane of the sample and the radius of curvature of the growth plate were measured in a lateral view for all samples (cf. Supplementary Material, Fig. 2). Based on a parametric finite element study (cf. supplementary material, section 1), the maximum permissible angle and curvature of the growth plate within the samples were determined. The criterion for inclusion was that the maximum stress within the growth plate should not deviate by more than 10 % compared to an ideally aligned, flat sample. Following this, samples showing an angular deviation greater than 8.25° or a radius of curvature smaller than 17.13 mm were excluded. A radius of 17.13 mm corresponds to a vertical deviation of 0.27 mm between the highest and lowest points across the sample (Shen et al., 2020).

A total of 140 samples were used for mechanical testing and 100 samples for the detailed histological examination. The distribution of the samples across individuals and growth plate types is given in Table 1.

The shear strain γ was calculated as

$$\gamma = \frac{C\theta}{t}, \quad (3)$$

where θ is the angle of twist and t the thickness of the growth plate (Young and Budynas, 2002).

The transition from purely elastic to inelastic deformation was identified by determining the inflection point (*IP*) (Holzapfel et al., 2000) (Fig. 3, A). After smoothing the data using the smoothing spline method with the smoothing parameter p = 1, the inflection point was determined as the point of the stress-strain curve $\tau(\gamma)$ showing the maximum slope, i.e. the maximum of the derivative $d\tau/d\gamma$ by using the numerical gradient function implemented in Matlab.

Since τ is only given by discrete values, the finite difference method is used to estimate the derivative $d\tau/d\gamma$ as

$$\frac{d\tau}{d\gamma} \approx \frac{\tau(\gamma + h) - F(\gamma - h)}{2h}, \quad (4)$$

where h is a small number representing small change in τ. The result of this is a vector containing $d\tau/d\gamma$ for each torsional stress value. The inflection point was then estimated by finding the maximum of $d\tau/d\gamma$. The last cycle of purely elastic deformation, being the last cycle before the cycle including the inflection point, was then extracted from each sample and used for further analysis. The ascending stress-strain curve was used to determine two shear moduli, namely the primary shear modulus (ME1), the gradient $d\tau/d\gamma$ at the beginning of the curve and the secondary shear modulus (ME2), the gradient $d\tau/d\gamma$ at the end of the curve (Fig. 3, B). The trapezoidal method was employed to calculate the area under the ascending curve for the total deformation energy. The dissipated energy was obtained by subtracting the area under the descending curve from the total deformation energy. Subsequently, the dissipated energy was divided by the total deformation energy to determine the energy ratio (MV1) (Fig. 3, C). The energy ratio serves as a metric for assessing the viscoelastic properties of the tested samples.

The destruction tests were also evaluated by calculating the torsional stress and shear strain γ (Equations (3)–(4)). In order to ascertain the stress at failure of the specimen, the maximum torsional stress τ_{max} (MF2) was identified. The requisite failure energy (MF1) was calculated using the trapezoidal method to determine the area under the curve up to the failure stress (Fig. 3, D). An overview of evaluation parameters and abbreviations can be found in Table 1.

Table 1
Overview over the mechanical and histological parameters and the groups used for statistical analyses. After each group name, the number of samples in the respective group for the mechanical test and the histological examination (in brackets) is indicated.

Parameter				
	Mechanical (M)	Elastic (ME)	ME1: primary shear modulus ME2: secondary shear modulus	
		Viscoelastic (MV)	MV1: energy ratio	
		Failure (MF)	MF1: failure energy MF2: maximum torsional stress τ_{max}	
	Histological (H)		H1: thickness of whole growth plate H2: thickness of hypertrophic zone H3: thickness of proliferative zone H4: thickness of resting zone H5: number of cells in hypertrophic zone H6: angle α between bone/hypertrophic zone interface and cell columns	
Groups	**Individuals (I)**	1 to 5	IND1 IND2 IND3 IND4 IND5	31 (17) 22 (19) 48 (20) 13 (23) 26 (21)
	Type	of growth plate	PF: proximal femur DF: distal femur PT: proximal tibia	23 (20) 71 (38) 46 (42)
	Anatomical location	within each growth plate	lat: lateral med: medial	48 (34) 49 (47)
	Testing velocity	of mechanical tests	low: 0.04°/s medium: 0.2°/s fast: 0.5°/s	32 73 35
			Total number of samples	140 (100)

2.4. Histological analysis

For histological analysis, samples were first fixed in a 4 % formalin solution for 48 h and subsequently decalcified using a 14 % EDTA solution over a period of 30 days. After decalcification, the samples were embedded in paraffin and sectioned into 7 μm thick slices. All sections were then stained with MOVAT pentachrome (MORPHISTO GmbH, Offenbach am Main, Germany).

Two histologic images were obtained for each sample using bright-field microscopy (DMI6000B, Leica Microsystems, Wetzlar, Germany) and *Leica Application Suite X (LAS X) software* (LAS X, *version 5.2.2,* Leica Microsystems). The thickness of the different growth plate zones – hypertrophic zone, proliferative zone, and resting zone – as well as the 'cell stack angle' between the bone-growth plate interface and the direction of the cell stacks were measured manually be the same experienced observer using the image processing program ImageJ (ImageJ 1.54j, U. S. National Institutes of Health, Bethesda, Maryland, USA, Fig. 4). Each measurement was repeated six times at different locations within each growth plate. Since a direction of the 'cell stack angle' could not be determined reasonably, it was defined to be $\leq 90°$. The number of cells

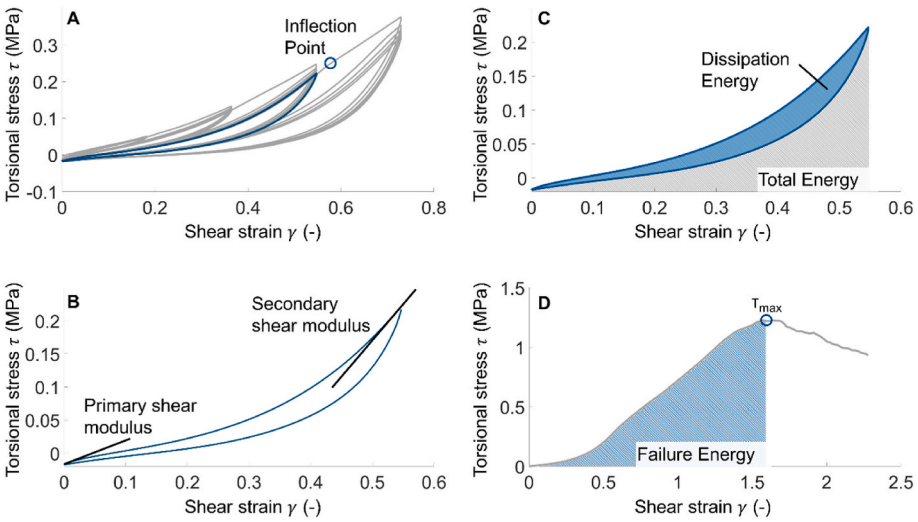

Fig. 3. Evaluation parameters for cyclic and failure testing. (A) The last complete elastic curve (blue) after the inflection point was used for analysis. (B) Primary (ME1) and secondary (ME2) shear moduli were measured at the start and end of the elastic curve. (C) The energy ratio (MV1) was calculated as dissipation energy (blue) over total energy (hatched area). (D) For failure tests, maximal torsional stress (τ_{max}, MF2) and failure energy (MF1) were determined. (For interpretation of the references to colour in this figure legend, the reader is referred to the Web version of this article.)

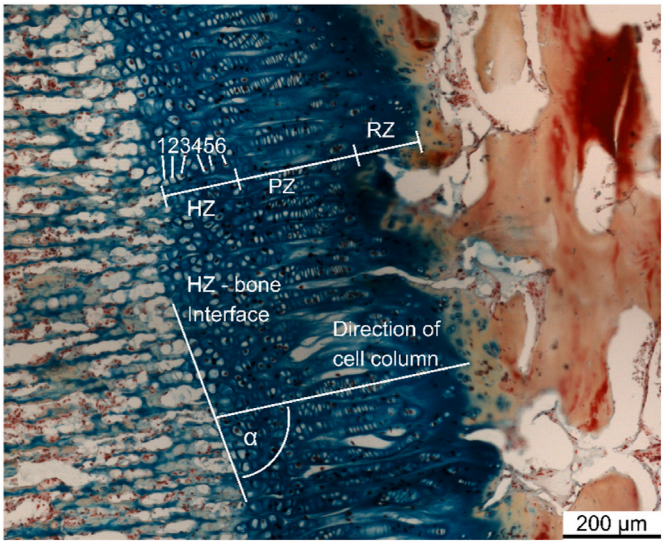

Fig. 4. Evaluation parameters H1 – H6 acc. to Table 1 from histological images: (H1) thickness of the growth plate (H2) thickness of the hypertrophic zone (HZ), (H3) proliferative zone (PZ), and (H4) resting zone (RZ); (H5) cell count in the HZ (counts 1–6); and (H6) angle α between the hypertrophic zone and bone interface and a cell column.

in a single cell column within the hypertrophic zone was counted manually at six different locations by the same observer.

2.5. Statistical methods

In order to prepare the data for statistical correlation analysis and hypothesis testing, the data was grouped according to the following characteristics: five distinct individuals, three different types of growth plates, the location within each growth plate (lateral and medial, Fig. 2) and the testing velocity. The objective of the statistical analysis was not to provide information about the population; rather, it was to examine the differences between the groups and the correlation of the parameters for the examined samples.

Initially, the normality of each group was assessed using the Anderson-Darling test. Based on these results, the appropriate statistical tests were selected to compare mean or median values among the groups. For two groups, if all were normally distributed, a two-sample *t*-test was applied. If at least one group was not normally distributed, the Mann-Whitney *U* test was used. This concerned the tests of the anatomical location, as well as the grouping according to the different types of growth plates at 0.04°/s and 0.5°/s. Although multiple samples per growth plate type were taken from the same individuals, exploratory analysis revealed no systematic differences between animals (see supplementary material, section 4). Therefore, samples were treated as independent. For comparisons involving more than two groups, ANOVA with an F-test and post-hoc multiple comparison tests were employed if all groups were normally distributed. Conversely, if at least one group was not normally distributed, the Kruskal-Wallis test along with post-

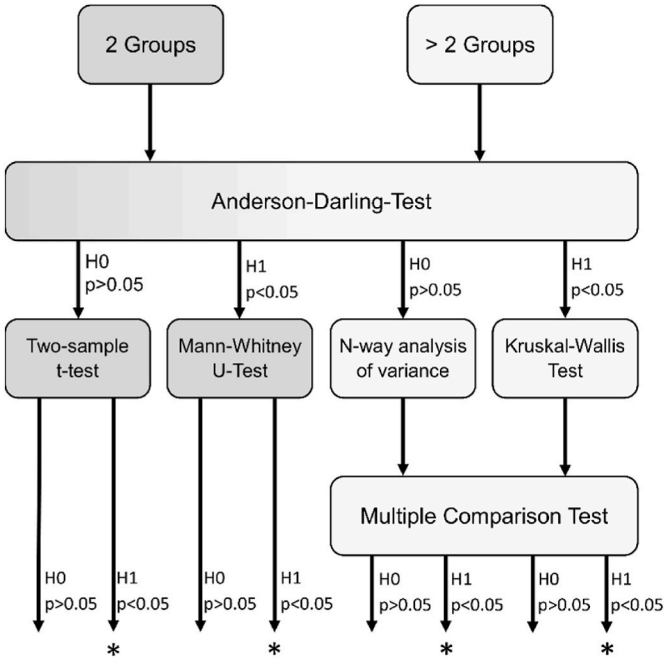

Fig. 5. Flowchart of statistical methods. Normal distribution was assessed using the Anderson-Darling test. Depending on distribution and number of groups, appropriate tests were selected to identify significant differences.

hoc multiple comparison tests were utilized. Fig. 5 gives an overview of the different statistical tests used and the conditions under which they were applied. The null hypothesis was rejected for all tests with a significance level of $p < 0.05$.

After outliers were identified using the interquartile range method, Spearman's rank test was employed to assess the correlation between mechanical test parameters and histological results, given that the majority of groups were not normally distributed. The statistical significance threshold was set at $p < 0.05$. All tests were conducted using MATLAB 2023a.

3. Results

3.1. Key results of mechanical testing

Table 2 illustrates significant differences between the different growth plates for each testing speed and between testing speeds itself. The analysis showed that there were significant differences in both the primary (ME1) and secondary (ME2) shear moduli across different growth plate types, although the energy ratio (MV1) did not change (Fig. 6). There was no significant difference between the median values of the primary shear modulus of the distal femoral and proximal tibial growth plates. However, the secondary shear modulus was significantly higher in the proximal tibial growth plate then in the distal femur (Fig. 6, A-B; Table 2). The proximal femoral growth plate demonstrated differences in the primary and the secondary shear moduli being significantly higher compared to the growth plates in the distal femur and the proximal tibia (Fig. 6, A-B; Table 2). No differences between the individuals, growth plate types, and anatomical positions within each growth plate were found in the results of the failure experiments (MF1). A comprehensive list of the complete results can be found in the supplementary material, section 4.

Table 2
Key results of mechanical testing. The table compares growth plate types (proximal femur (PF), proximal tibia (PT), distal femur (DF)) at different testing velocities. For the primary shear modulus (ME1), secondary shear modulus (ME2), energy ratio (MV1), and failure energy (MF1), median [IQR] values are shown. Statistical tests used: F-test (ANOVA, F) or Kruskal-Wallis test (H) for >2 groups, unpaired *t*-test (t) or Mann-Whitney *U* test (U) for 2 groups. Significant differences ($p < 0.05$) are marked with an asterisk (*).

		ME1 (MPa)	ME2 (MPa)	MV1 (–)	MF1 (MJ)
Type of growth plate					
0.04 °/s	**PF**	0.93 [1.8]	1.56 [1.27]	0.3 [0.15]	0.42 [0.34]
	PT	1.1 [0.86]	0.99 [1.06]	0.29 [0.12]	0.46 [0.58]
	PF vs. PT	U, -	t, -	t, -	U, -
0.2 °/s	**DF**	1.12 [1.37]	1.32 [1.16]	0.31 [0.09]	0.51 [0.41]
	PF	2.55 [2.99]	3.23 [2.39]	0.33 [0.13]	0.44 [0.2]
	PT	1.17 [1.36]	2.08 [1.48]	0.34 [0.1]	0.36 [0.24]
	DF vs. PF	H, *	H, *	F, -	H, -
	DF vs. PT	H, -	H, *	F, -	H, *
	PF vs. PT	H, *	H, -	F, -	H, -
0.5 °/s	**PF**	1.79 [1.89]	4.14 [1.61]	0.29 [0.09]	0.31 [0.25]
	PT	1.15 [1.69]	1.89 [0.9]	0.25 [0.12]	0.33 [0.36]
	PF vs. PT	U, -	t, *	t, -	U, -
Testing speed					
	0.04 °/s	1.09 [1.30]	1.27 [1.05]	0.3 [0.12]	0.31 [0.29]
	0.2 °/s	0.91 [0.84]	2.12 [0.79]	0.3 [0.09]	0.42 [0.46]
	0.5 °/s	1.43 [2.07]	2.24 [1.75]	0.26 [0.1]	0.4 [0.29]
	0.04 °/s vs. 0.2 °/s	H, -	H, -	F, -	H, -
	0.04 °/s vs. 0.5 °/s	H, -	H, *	F, -	H, -
	0.2 °/s vs. 0.5 °/s	H, -	H, *	F, -	H, -

3.2. Key results of histological analyses

The results of the evaluation of the histological parameters are shown in Table 3. The evaluation revealed that there were no significant differences between the distal femoral and proximal tibial growth plates. This was observed to be the case for all histological parameters that were evaluated, e.g. the thickness of the individual zones and the entire growth plate, as well as the number of cells and the angle of the cell stacks. In contrast, the hypertrophic zone (H2) proximal femoral growth plate was significantly thinner compared to both, the distal femoral and proximal tibial plates (Table 3). The proliferative zone also differed significantly between the two femoral growth plates, with the proximal femoral growth plate having a thinner proliferative zone than the distal femoral growth plate. There were no significant differences in the resting zone thickness or cell column angle (Table 3).

3.3. Differences between testing velocities

Further grouping by testing velocity showed that the energy ratio (MV1) did not differ across velocities. However, the secondary shear modulus (ME2) was significantly higher at 0.5°/s than at 0.2°/s or 0.04°/s, while the primary shear modulus (ME1) remained unchanged. The evaluation of the failure energy (Fig. 3, D) revealed no differences between the various growth plate types (Table 2).

Spearman analyses yielded a negative correlation between the thickness of the hypertrophic zone and the primary shear modulus for all data pooled. The correlation was non-significant with a Spearman's rho $\rho = 0.07$ at a testing velocity of $0.04°/s$ ($p = 0.752$), yet getting moderately stronger and highly significant at increasing test velocity, decreasing from $\rho = -0.30$ at $0.2°/s$ ($p = 0.02$) to $\rho = -0.47$ at $0.5°/s$ ($p = 0.01$).

Negative correlations were also found between the angle of the cell columns (Fig. 4) and the secondary shear modulus, indicating that steeper angles corresponded with an increased shear modulus. This correlation also became stronger as the test speed increased. The correlation coefficient was $\rho = -0.14$ at the slowest of the observed testing velocities of $0.04°/s$ ($p = 0.515$), decreased to $\rho = -0.22$ at $0.2°/s$ ($p = 0.09$), and finally reached $\rho = -0.43$ at $0.5°/s$ ($p = 0.02$).

4. Discussion

4.1. Growth plate types differ more than individuals or anatomical locations under torsion

The mechanical properties under torsional loading varied primarily between growth plate types, with no significant differences between individuals or anatomical subregions (medial vs. lateral) (Table 2, Fig. 6). This consistency between individuals likely results from the homogeneity in breed, age, and farming conditions. A broader study would be needed to confirm this across a more diverse population. The lack of regional differences contrasts with Fischenich et al. (2022), who reported variation in compressive stiffness within the proximal tibial plate. This discrepancy might stem from the different loading modes studied—torsion versus compression. The dissipation ratio, used to assess viscoelasticity, showed no significant differences, indicating similar viscoelastic behavior across all samples.

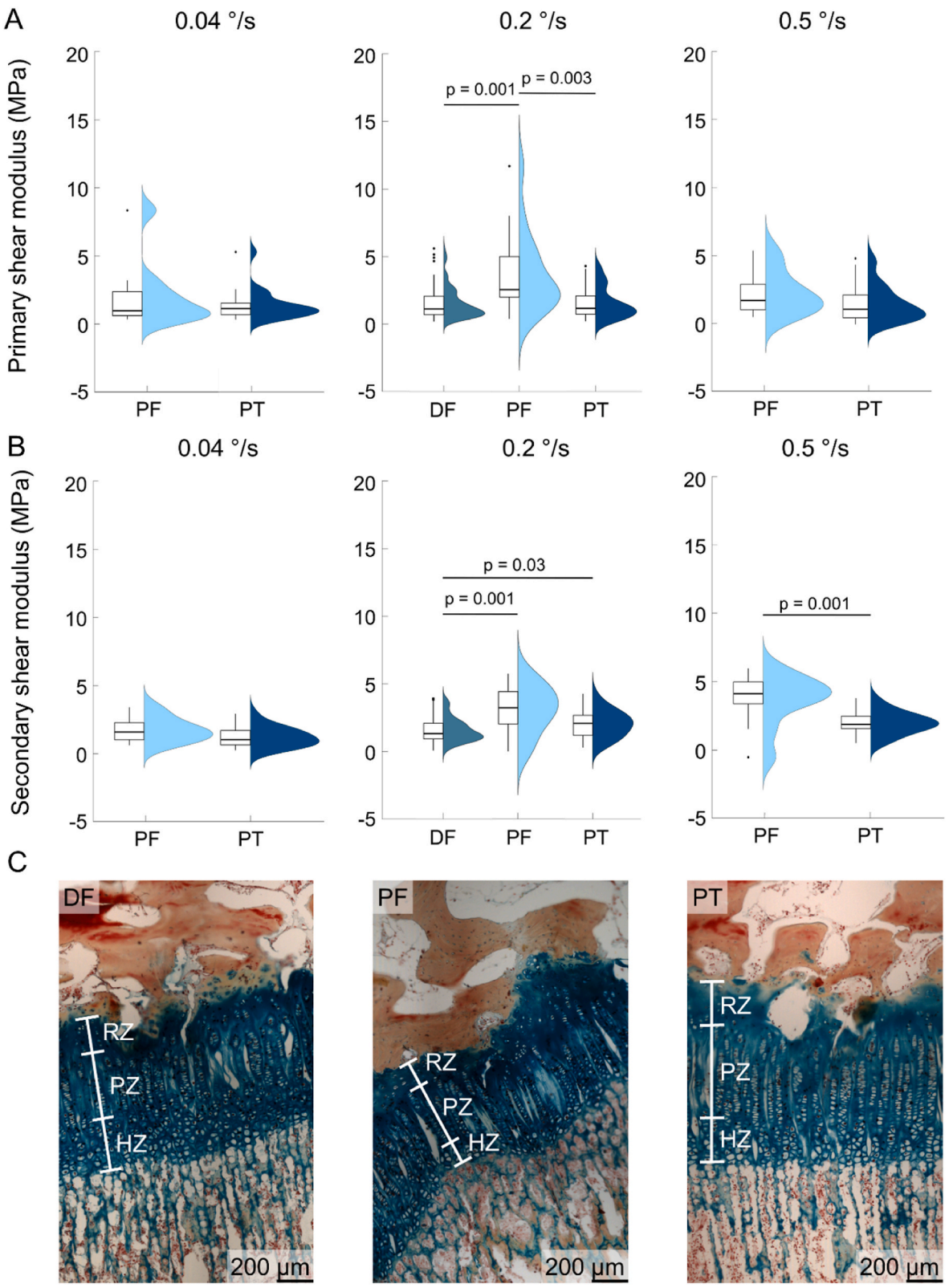

Fig. 6. Shear moduli and histology results for different growth plate types. (A) Primary shear modulus (ME1) and (B) secondary shear modulus (ME2) at three testing velocities. (C) Histological images show a significantly thinner hypertrophic zone in PF compared to PT and DF (median [IQR]: PF 113.12 [55.13] µm, PT 154.74 [45.76] µm, $p = 0.009$; DF 154.1 [40.67] µm, $p = 0.0003$).

Table 3
Key results of histological analysis. The table compares growth plate types (proximal femur (PF), proximal tibia (PT), distal femur (DF)). Parameters shown are total growth plate thickness (H1), thickness of the hypertrophic (H2), proliferative (H3), and resting (H4) zones, number of cells in the hypertrophic zone (H5), and the angle between the hypertrophic zone–bone interface and the cell columns (H6). Statistical tests used: F-test (ANOVA, F) or Kruskal-Wallis test (H) for >2 groups. Significant differences ($p < 0.05$) are indicated by an asterisk (*).

	H1 (μm)	H2 (μm)	H3 (μm)	H4 (μm)	H5 (N)	H6 (°)
DF	699.1 [228]	161.8 [49.1]	369.5 [119.6]	162.4 [244.5]	7.5 [1.58]	74.9 [7.31]
PF	584.0 [107.7]	121.3 [49.3]	304.2 [104.9]	160.4 [142.8]	7.25 [1.92]	71.4 [10.4]
PT	636.7 [172.1]	151.5 [45.4]	338.4 [120.4]	136.1 [142.0]	7.75 [1.5]	75.5 [7.45]
DF vs. PF	H, *	H, *	H, *	H, -	F, -	H, -
DF vs. PT	H, -	H, -	H, -	H, -	F, -	H, -
PF vs. PT	H, -	H, *	H, -	H, -	F, *	H, -

4.2. Proximal femoral plate shows higher shear stiffness than others

The proximal femoral growth plate displayed substantially higher shear moduli than the distal femoral and proximal tibial plates, which did not differ significantly from each other (Table 2). Specifically, the primary shear modulus of the proximal femur exceeded that of the tibia and distal femur by ~47–60 % and ~43 %, respectively. The secondary shear modulus showed similar differences. These findings align with prior studies suggesting that the proximal femur experiences higher shear forces (Sadeghian et al., 2020) and a larger curvature radius (Kandzierski et al., 2012; Yadav et al., 2021). Bone geometry and localized growth rates may also contribute to the elevated mechanical resistance (Villemure and Stokes, 2009; Yadav et al., 2016).

4.3. Zonal structure correlates with mechanical differences

The primary shear modulus correlated inversely with the thickness of the hypertrophic zone—thinner zones yielded higher moduli, especially at higher testing speeds. In contrast, the secondary shear modulus correlated with the angle of the cell columns, with more oblique orientations showing higher stiffness. These findings likely relate to the growth plate's zonal architecture. While articular cartilage properties depend largely on collagen II content and orientation (Fischenich et al., 2020; Wang et al., 2020), growth plate mechanics are more influenced by zonal organization and ossification processes (Ağırdil, 2020; Amini et al., 2012). Collagen type X becomes dominant in the hypertrophic zone and may contribute to its lower stiffness (Gibson et al., 1996; Tiffany and Harley, 2022). These mechanical differences are supported by structural alignment and collagen distribution (Speer, 1982; Prein et al., 2016).

4.4. Proximal femoral plate fails at higher torsional stress

To relate torsional results to existing shear data, torsional failure stress was calculated. Shen et al. (2020) found higher simple shear stress in the proximal femoral plate of young pigs compared to distal femur and tibia. This trend was mirrored in our torsional results at 0.02°/s, with the proximal femoral plate failing at 1.24 MPa versus ~0.76–0.77 MPa in the other plates. However, these differences were not observed at higher testing speeds or in failure energy. Variations between studies likely stem from differences in pig age (30 vs. 20 weeks), loading rates, and small sample sizes. Our stress values were generally lower than those reported by Shen et al. (2020) and by Niehoff et al. (2004) in rats, possibly due to species- and age-related factors. Failure energy was significantly higher in the distal femoral plate than the proximal tibia, likely due to greater deformation capacity at similar stress levels—consistent with its lower secondary modulus.

4.5. Testing velocity affects secondary, but not primary shear modulus

Testing speed had little effect on the primary shear modulus but significantly influenced the secondary modulus. At the highest speed, the secondary modulus increased in both the proximal tibial and femoral plates (Table 2). This modulus reflects tissue behavior near failure and suggests that faster loading increases resistance to deformation. This may reflect a protective mechanism under rapid physiological loads, limiting harmful deformations (Xie et al., 2020). While testing used displacement control, in vivo loading is force-driven, so higher stiffness under faster loads may help maintain structural integrity.

4.6. Growth plates tolerate high torsional angles

Failure occurred at angles exceeding 20°, indicating a higher torsional deformation capacity than previously reported. Although literature data on torsional failure in growth plates is sparse, torsion is implicated in Salter-Harris Type II injuries (Salter and Harris, 1963; Jones et al., 2017). The large failure angles observed suggest that growth plates can endure more torsional strain than generally assumed, offering new insights into injury mechanisms in growing bones.

4.7. Limitations

The main limitation of this study is the small sample size, with only five individuals examined. Thus, the findings are not fully representative and apply only to the samples tested. Nonetheless, due to limited data on growth plate behavior under torsional loading, these results add valuable insight. Future studies with larger sample sizes are needed to improve representativeness and strengthen conclusions.

Samples were treated as independent observations in statistical analyses despite multiple samples from the same individual. This may overestimate significance due to within-subject correlation. However, exploratory analyses showed no consistent inter-individual differences and considerable variation within individuals, supporting this approach for this exploratory study. Future work could benefit from hierarchical models like mixed-effects models.

The exact age and sex of the porcine specimens were not recorded; they were approximately 30 weeks old and either castrated males or females. No consistent material property differences were observed (see Supplementary Material, Section 4). However, the study was not powered to detect sex effects, which remain a limitation.

Collagen fiber orientation was unknown due to staining limitations. Research on collagen content and orientation in the growth plate is scarce, especially regarding their effect on material properties and zonal biomechanics. This gap highlights the need for further studies to clarify collagen's role in growth plate mechanics.

Mechanical tests were performed in torsion without controlled normal forces, though minor normal forces may have occurred due to geometric and fixation variations. Further experiments are necessary to explore combined loading effects.

5. Conclusion

This study provides a detailed analysis of the morpho-mechanical behavior of porcine growth plate tissue under torsional shear loading, addressing a significant gap in the existing literature. While there has been limited research on shear properties of the growth plate, studies on torsional loading have been notably absent until now. Significant variations in shear moduli were observed across different growth plate types and testing velocities, with the proximal femoral growth plate

demonstrating higher mechanical stiffness than the distal femur and proximal tibia. Histological analysis showed differences in zone thickness, particularly a thinner hypertrophic zone in the proximal femur. Correlations between tissue microstructure and mechanical properties were identified, suggesting that increased testing velocity amplifies the influence of structural features like zone thickness and cell column orientation on mechanical response.

CRediT authorship contribution statement

L. Hucke: Writing – original draft, Investigation, Data curation, Methodology, Formal analysis, Conceptualization. **G.Q. Teixeira:** Supervision, Writing – review & editing, Methodology. **A. Seitz:** Writing – review & editing, Resources, Supervision. **A.J. Gámez:** Supervision, Writing – review & editing, Resources. **A. Huß:** Supervision, Funding acquisition, Writing – review & editing, Resources. **N. Hammer:** Writing – review & editing, Resources, Supervision. **A. Wittek:** Writing – review & editing, Methodology, Supervision, Conceptualization. **J.A. Niestrawska:** Writing – review & editing, Supervision, Methodology, Writing – original draft, Project administration, Conceptualization.

Declaration of AI and AI-assisted technologies in the writing process

During the preparation of this work the authors used DeepL Translate and DeepL Write in order to check on the language used and improve the readability of the work. The tools did not interpret the data or draw scientific conclusions. After using these tools, the authors reviewed and edited the content as needed and take full responsibility for the content of the publication.

Declaration of competing interest

The authors declare that they have no known competing financial interests or personal relationships that could have appeared to influence the work reported in this paper.

Acknowledgements

We would like to express our sincere gratitude to Matthias Walluch from Anton Paar for his invaluable assistance in setting up the experiments and Anton Paar for providing the rheometer used in this study. Their expertise and support were instrumental in ensuring the successful completion of our experimental work.

The research stay of Lucie Hucke at the Division of Macroscopic and Clinical Anatomy, Medical University of Graz was funded by the “Forschungsstipendien für Doktorandinnen und Doktoranden”, ID 57647578, a travel scholarship for research stays of PhD students, of the Deutscher Akademischer Austausch Dienst (German Academic Exchange Service).

Appendix A. Supplementary data

Supplementary data to this article can be found online at https://doi.org/10.1016/j.jmbbm.2025.107160.

Data availability

Data will be made available on request.

References

Ağırdil, Y., 2020. The growth plate: a physiologic overview. EFORT Open Rev. 5, 498–507. https://doi.org/10.1302/2058-5241.5.190088.

Alonso, G., Yawny, A., Bertolino, G., 2022. How do bones grow? A mathematical description of the mechanobiological behavior of the epiphyseal plate. Biomech. Model. Mechanobiol. 21, 1585–1601. https://doi.org/10.1007/s10237-022-01608-y.

Amini, S., Mortazavi, F., Sun, J., Levesque, M., Hoemann, C.D., Villemure, I., 2012. Stress relaxation of swine growth plate in semi-confined compression: depth dependent tissue deformational behavior versus extracellular matrix composition and collagen fiber organization. Biomech. Model. Mechanobiol. 12, 67–78. https://doi.org/10.1007/s10237-012-0382-y.

Carriero, A., Jonkers, I., Shefelbine, S.J., 2011. Mechanobiological prediction of proximal femoral deformities in children with cerebral palsy. Comput. Methods Biomech. Biomed. Eng. 14, 253–262. https://doi.org/10.1080/10255841003682505.

Castro-Abril, H.A., Gutiérrez, M.L., Garzón-Alvarado, D.A., 2016. Proximal femoral growth plate mechanical behavior: comparison between different developmental stages. Comput. Biol. Med. 76, 192–201. https://doi.org/10.1016/j.compbiomed.2016.07.011.

Cone, S.G., Warren, P.B., Fisher, M.B., 2017. Rise of the pigs: utilization of the porcine model to study musculoskeletal biomechanics and tissue engineering during skeletal growth. Tissue Eng. C Methods 23, 763–780. https://doi.org/10.1089/ten.TEC.2017.0227.

D'Andrea, C.R., Alfraihat, A., Singh, A., Anari, J.B., Cahill, P.J., Schaer, T., Snyder, B.D., Elliott, D., Balasubramanian, S., D'Andrea, C.R., 2021. Part 2. Review and meta-analysis of studies on modulation of longitudinal bone growth and growth plate activity: a micro-scale perspective. Journal of Orthopaedic Research\textregistered 39, 919–928. https://doi.org/10.1002/jor.24992.

Eckstein, K.N., Thomas, S.M., Scott, A.K., Neu, C.P., Hadley-Miller, N.A., Payne, K.A., Ferguson, V.L., 2022. The heterogeneous mechanical properties of adolescent growth plate cartilage: a study in rabbit. J. Mech. Behav. Biomed. Mater. 128, 105102. https://doi.org/10.1016/j.jmbbm.2022.105102.

Farr, S., Alrabai, H.M., Meizer, E., Ganger, R., Radler, C., 2018. Rebound of frontal plane malalignment after tension band plating. Journal of pediatric orthopedics 38, 365–369. https://doi.org/10.1097/BPO.0000000000000846.

Fischenich, K.M., Wahlquist, J.A., Wilmoth, R.L., Cai, L., Neu, C.P., Ferguson, V.L., 2020. Human articular cartilage is orthotropic where microstructure, micromechanics, and chemistry vary with depth and split-line orientation. Osteoarthr. Cartil. 28, 1362–1372. https://doi.org/10.1016/j.joca.2020.06.007.

Fischenich, K.M., Schneider, S.E., Neu, C.P., Payne, K.A., Ferguson, V.L., 2022. Material properties and strain distribution patterns of bovine growth plate cartilage vary with anatomic location and depth. J. Biomech. 134, 111013. https://doi.org/10.1016/j.jbiomech.2022.111013.

Gibson, G., Lin, D.L., Francki, K., Caterson, B., Foster, B., 1996. Type X collagen is colocalized with a proteoglycan epitope to form distinct morphological structures in bovine growth cartilage. Bone 19, 307–315. https://doi.org/10.1016/S8756-3282(96)00222-0.

Giesche, F., Stief, F., Groneberg, D.A., Wilke, J., 2021. Effect of unplanned athletic movement on knee mechanics: a systematic review with multilevel meta-analysis. Br. J. Sports Med. 55, 1366–1378. https://doi.org/10.1136/bjsports-2021-103933.

Gottliebsen, M., Møller-Madsen, B., Stødkilde-Jørgensen, H., Rahbek, O., 2013. Controlled longitudinal bone growth by temporary tension band plating: an experimental study. The bone & joint journal 95-B, 855–860. https://doi.org/10.1302/0301-620X.95B6.29327.

Gottliebsen, M., Shiguetomi-Medina, J.M., Rahbek, O., Møller-Madsen, B., 2016. Guided growth: mechanism and reversibility of modulation. Journal of children's orthopaedics 10, 471–477. https://doi.org/10.1007/s11832-016-0778-9.

Heyland, M., Deppe, D., Reisener, M.J., Damm, P., Taylor, W.R., Reinke, S., Duda, G.N., Trepczynski, A., 2023. Lower-limb internal loading and potential consequences for fracture healing. Front. Bioeng. Biotechnol. 11, 1284091. https://doi.org/10.3389/fbioe.2023.1284091.

Holzapfel, G.A., Gasser, T.C., Ogden, R.W., 2000. A new constitutive framework for arterial wall mechanics and a comparative study of material models. J. Elasticity 61, 1–48. https://doi.org/10.1023/A:1010835316564.

Hucke, L., Holder, J., van Drongelen, S., Stief, F., Gámez, A.J., Huß, A., Wittek, A., 2023. Influence of tension-band plates on the mechanical loading of the femoral growth plate during guided growth due to coronal plane deformities. Front. Bioeng. Biotechnol. 11, 1165963. https://doi.org/10.3389/fbioe.2023.1165963.

Innocenti, B., 2022. Biomechanics of the knee joint. In: Innocenti, B., Galbusera, F. (Eds.), Human Orthopaedic Biomechanics: Fundamentals, Devices and Applications. Academic Press, London, pp. 239–263.

Jones, C., Wolf, M., Herman, M., 2017. Acute and chronic growth plate injuries. Pediatr. Rev. 38, 129–138. https://doi.org/10.1542/pir.2015-0160.

Kandzierski, G., Matuszewski, L., Wójcik, A., 2012. Shape of growth plate of proximal femur in children and its significance in the aetiology of slipped capital femoral epiphysis. Int. Orthop. 36, 2513–2520. https://doi.org/10.1007/s00264-012-1699-y.

Koller, W., Wallnöfer, E., Holder, J., Kranzl, A., Mindler, G., Baca, A., Kainz, H., 2024. ESMAC best paper award 2023: increased knee flexion in participants with cerebral palsy results in altered stresses at the distal femoral growth plate compared to a typically developing cohort. Gait Posture 113, 158–166. https://doi.org/10.1016/j.gaitpost.2024.06.012.

Mirtz, T.A., Chandler, J.P., Eyers, C.M., 2011. The effects of physical activity on the epiphyseal growth plates: a review of the literature on normal physiology and clinical implications. Journal of clinical medicine research 3, 1–7. https://doi.org/10.4021/jocmr477w.

Niehoff, A., Kersting, U.G., Zaucke, F., Morlock, M.M., Brüggemann, G.-P., 2004. Adaptation of mechanical, morphological, and biochemical properties of the rat growth plate to dose-dependent voluntary exercise. Bone 35, 899–908. https://doi.org/10.1016/j.bone.2004.06.006.

Perry, J., Burnfield, J., 2010. Gait Analysis: Normal and Pathological Function, second ed. Trafford, Canada.
Prein, C., Warmbold, N., Farkas, Z., Schieker, M., Aszodi, A., Clausen-Schaumann, H., 2016. Structural and mechanical properties of the proliferative zone of the developing murine growth plate cartilage assessed by atomic force microscopy. Matrix Biol. : journal of the International Society for Matrix Biology 50, 1–15. https://doi.org/10.1016/j.matbio.2015.10.001.
Sadeghian, S.M., Lewis, C.L., Shefelbine, S.J., 2020. Predicting growth plate orientation with altered hip loading: potential cause of cam morphology. Biomech. Model. Mechanobiol. 19, 701–712. https://doi.org/10.1007/s10237-019-01241-2.
Sadeghian, S.M., Lewis, C.L., Shefelbine, S.J., 2023. Can pelvic tilt cause cam morphology? A computational model of proximal femur development mechanobiology. J. Biomech. 157, 111707. https://doi.org/10.1016/j.jbiomech.2023.111707.
Salter, R.B., Harris, W.R., 1963. Injuries involving the epiphyseal plate. JBJS 45, 587 https://doi.org/aspx.
Sergerie, K., Lacoursière, M.-O., Lévesque, M., Villemure, I., 2009. Mechanical properties of the porcine growth plate and its three zones from unconfined compression tests. J. Biomech. 42, 510–516. https://doi.org/10.1016/j.jbiomech.2008.11.026.
Shen, M., Liu, S., Jin, X., Mao, H., Zhu, F., Saif, T., Zhou, R., Fan, H., Begeman, P.C., Chou, C.C., Yang, K.H., 2020. Porcine growth plate experimental study and estimation of human pediatric growth plate properties. J. Mech. Behav. Biomed. Mater. 101, 103446. https://doi.org/10.1016/j.jmbbm.2019.103446.
Speer, Donald P., 1982. Collagenous architecture of the growth plate and perichondrial ossification groove. J. Bone Joint Surg. 64 (3), 399–407.
Stamos, P.A., Berthaume, M.A., 2021. The effects of femoral metaphyseal morphology on growth plate biomechanics in juvenile chimpanzees and humans. Interface focus 11. https://doi.org/10.1098/rsfs.2020.0092.
Stamos, P.A., Weaver, T.D., 2020. Ontogeny of the distal femoral metaphyseal surface and its relationship to locomotor behavior in hominoids. Am. J. Phys. Anthropol. 172, 462–474. https://doi.org/10.1002/ajpa.24036.
Stevens, P.M., 2007. Guided growth for angular correction: a preliminary series using a tension band plate. Journal of pediatric orthopedics 27, 253–259. https://doi.org/10.1097/BPO.0b013e31803433a1.
Stief, F., Holder, J., Böhm, H., Meurer, A., 2021. Dynamic analysis of joint loading due to leg axis deformity in the frontal plane : relevance of instrumented gait analysis. Dynamische Analyse der Gelenkbelastung bei Beinachsendeformitäten in der Frontalebene : Stellenwert der instrumentellen Ganganalyse Orthopä 50, 528–537. https://doi.org/10.1007/s00132-021-04121-9.
Sun, X., Wu, W., Zhang, R., Qu, H., Wang, J., Xu, K., Fang, L., Xu, L., Jiang, R., 2022. Mechanical response and in-situ deformation mechanism of cortical bone materials under combined compression and torsion loads. PLoS One 17, e0271301. https://doi.org/10.1371/journal.pone.0271301.
Thomson, A., 1902. The relation of structure and function as illustrated by the form of the lower epiphysial suture of the femur. Journal of Anatomy and Physiology 36, 95–105.
Tiffany, A.S., Harley, B.A.C., 2022. Growing pains: the need for engineered platforms to study growth plate biology. Adv. Healthcare Mater. 11, e2200471. https://doi.org/10.1002/adhm.202200471.
Villemure, I., Stokes, I.A.F., 2009. Growth plate mechanics and mechanobiology. A survey of present understanding. J. Biomech. 42, 1793–1803. https://doi.org/10.1016/j.jbiomech.2009.05.021.
Wang, C., Brisson, B.K., Terajima, M., Li, Q., Hoxha, K., Han, B., Goldberg, A.M., Sherry Liu, X., Marcolongo, M.S., Enomoto-Iwamoto, M., Yamauchi, M., Volk, S.W., Han, L., 2020. Type III collagen is a key regulator of the collagen fibrillar structure and biomechanics of articular cartilage and meniscus. Matrix Biol. : journal of the International Society for Matrix Biology 85–86, 47–67. https://doi.org/10.1016/j.matbio.2019.10.001.
Wosu, R., Sergerie, K., Lévesque, M., Villemure, I., 2012. Mechanical properties of the porcine growth plate vary with developmental stage. Biomech. Model. Mechanobiol. 11, 303–312. https://doi.org/10.1007/s10237-011-0310-6.
Xie, M., Gol'din, P., Herdina, A.N., Estefa, J., Medvedeva, E.V., Li, L., Newton, P.T., Kotova, S., Shavkuta, B., Saxena, A., Shumate, L.T., Metscher, B.D., Großschmidt, K., Nishimori, S., Akovantseva, A., Usanova, A.P., Kurenkova, A.D., Kumar, A., Arregui, I.L., Tafforeau, P., Fried, K., Carlström, M., Simon, A., Gasser, C., Kronenberg, H.M., Bastepe, M., Cooper, K.L., Timashev, P., Sanchez, S., Adameyko, I., Eriksson, A., Chagin, A.S., 2020. Secondary ossification center induces and protects growth plate structure. eLife 9. https://doi.org/10.7554/eLife.55212.
Yadav, P., Shefelbine, S.J., Gutierrez-Farewik, E.M., 2016. Effect of growth plate geometry and growth direction on prediction of proximal femoral morphology. J. Biomech. 49, 1613–1619. https://doi.org/10.1016/j.jbiomech.2016.03.039.
Yadav, P., Fernández, M.P., Gutierrez-Farewik, E.M., 2021. Influence of loading direction due to physical activity on proximal femoral growth tendency. Med. Eng. Phys. 90, 83–91. https://doi.org/10.1016/j.medengphy.2021.02.008.
Young, W.C., Budynas, R.G., 2002. Roark's Formulas for Stress and Strain, seventh ed. McGraw-Hill, New York, NY, p. 852.
Zhang, X., Zhang, S., Wang, T., 2022. How the mechanical microenvironment of stem cell growth affects their differentiation: a review. Stem Cell Res. Ther. 13, 415. https://doi.org/10.1186/s13287-022-03070-0.